SGRB rate from Yonetoku relation for SGRB and the detectability of GW in O2 of a-LIGO/a-Virgo

2016.12.05
7 years of MAXI
Takashi Nakamura
Kyoto University

First of all

- Before O1 of aLIGO , the most relevant GW source was Neutron Star (NS)-NS mergers although the first directly detected GW source is Binary BH-BH (BBH) merger.

Almost everybody was surprised by ～30-30 solar mass BH merger event.

However we predicted $30M_{sun}$-$30M_{sun}$ BBH in 2014.

What is O1(Observing Run 1)

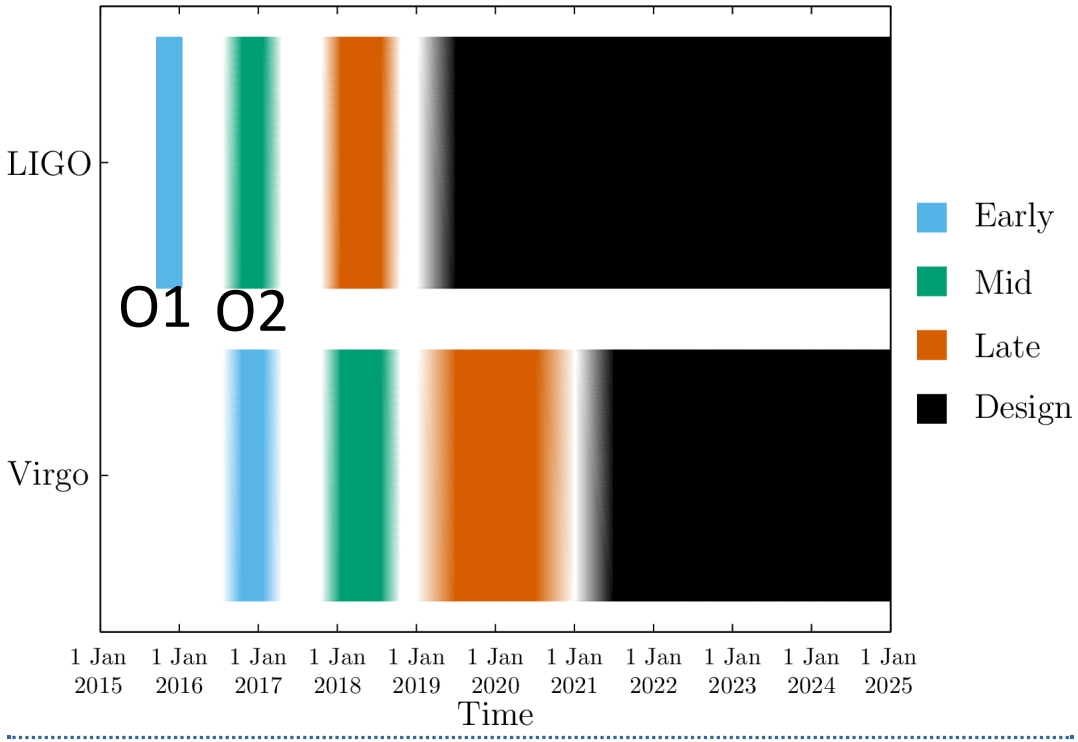

In O1 GWs from two BBH and one candidate were detected . Especially GW150914 is the first one with $\sim 30M_{sun}$ --$30M_{sun}$ BH

A plausible time-line for how LIGO and Virgo detectors will operate over the coming decade. Dates become more uncertain the further they are in the future. The colored bars correspond to observing runs, with the colors matching those in the sensitivity plots above. Between observing runs, we work on tuning our detectors to improve their sensitivity, and have engineering runs where we test the instruments and check that we understand how they behave while running.

Abbott et al. arXiv:1304.0670

Expected sensitivity

Abbott et al. arXiv:1304.0670

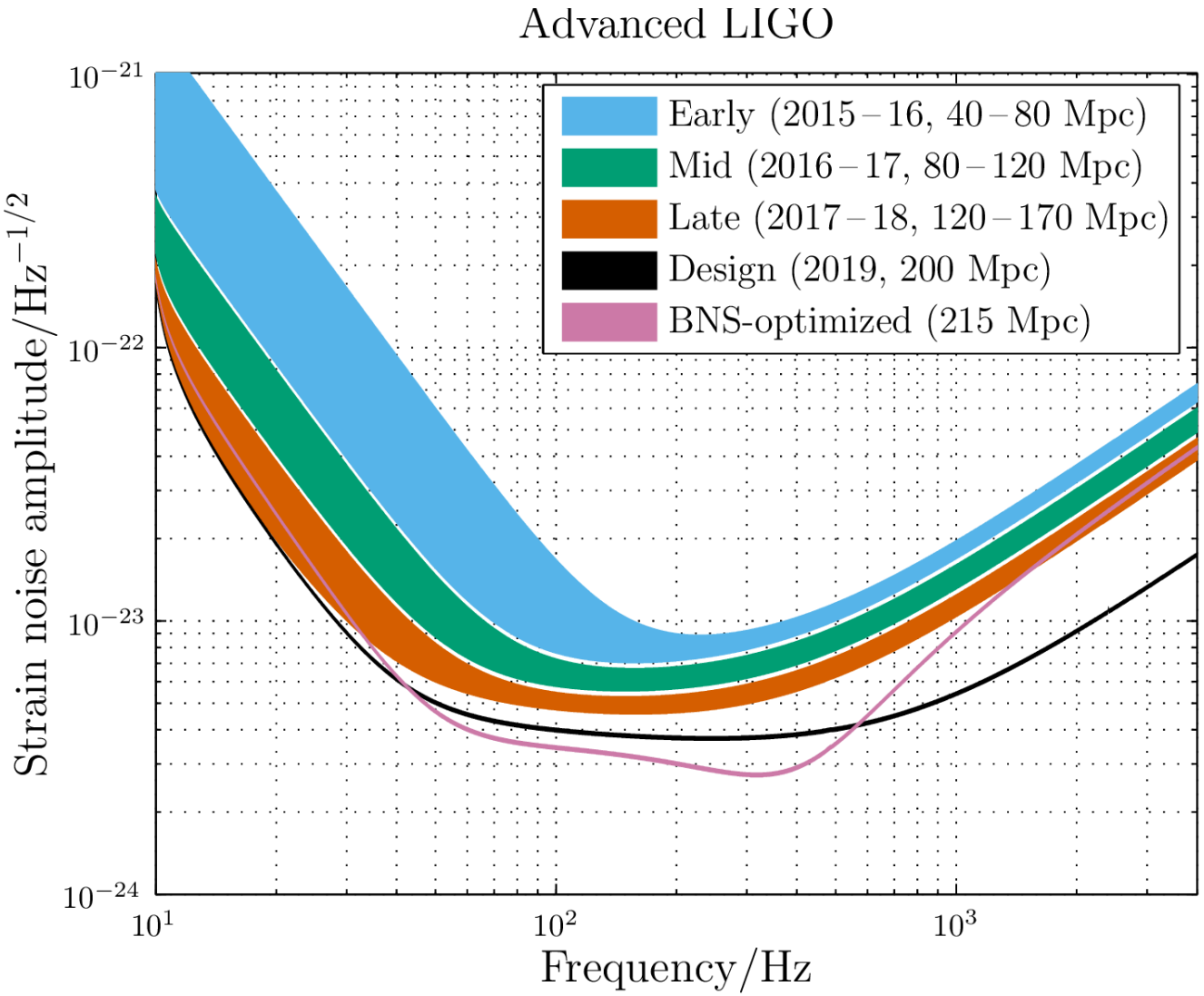

Abbott et al. arXiv:1304.0670

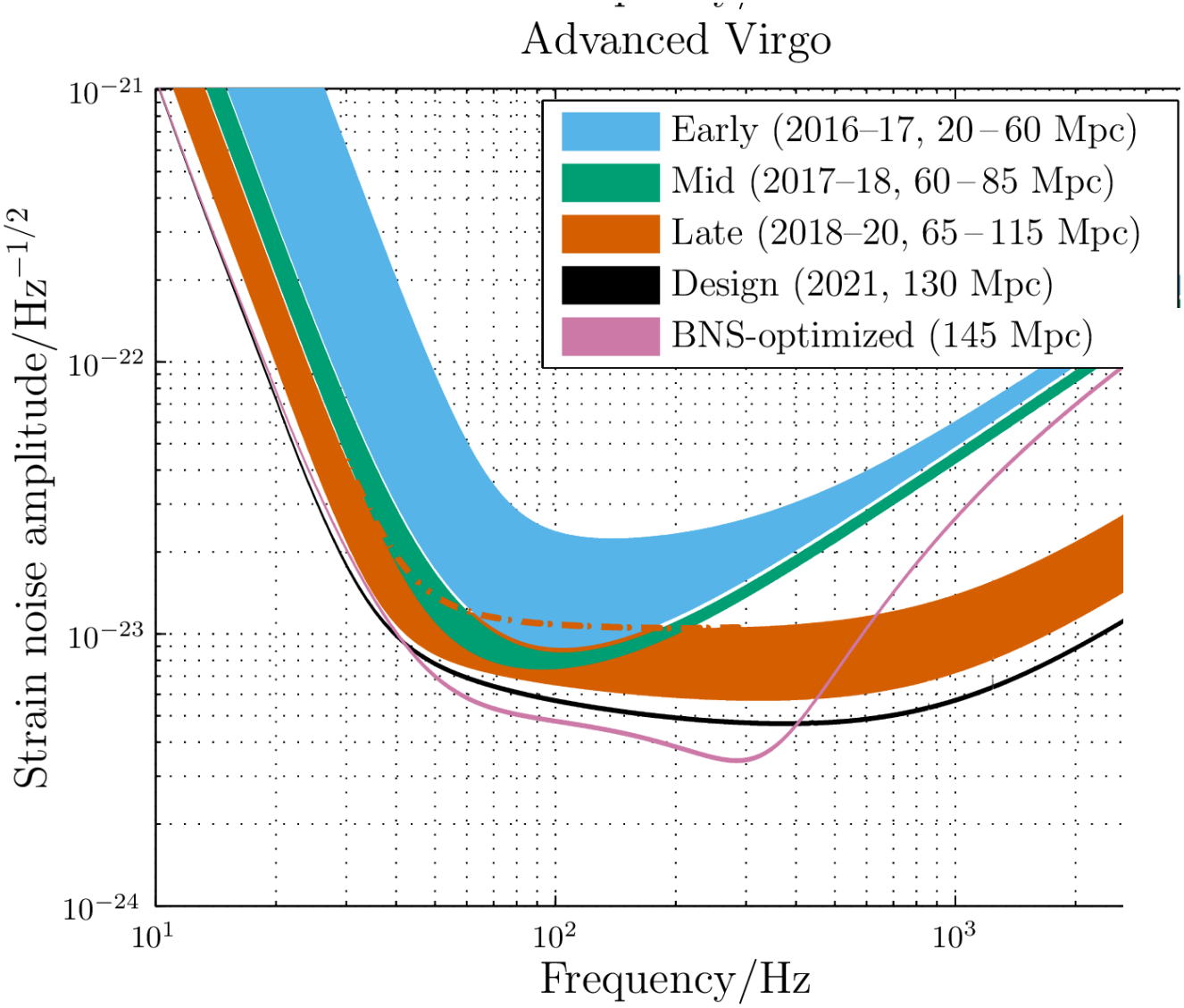

30 + 30 solar mass BHs

Interesting target for three reasons:

Inspiral and ringdown phases have roughly equal SNRs, so provides good test of GR

If population III stars (formed at redshifts 5-10) exist, these might be a substantial fraction.

Perhaps we will detect several of them in the first aLIGO data run O1, this September!

Nakano Talk

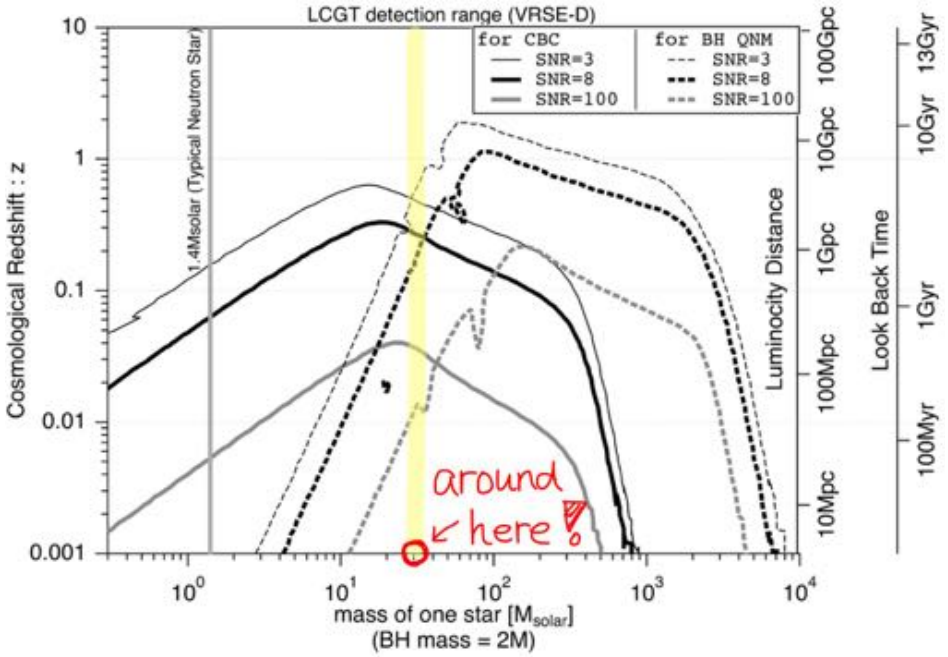

Summary talk of GWPAW2015(June) by Bruce Allen

30 M_{sun} comes from Kinugawa et al. 2014

Pop III stars = the first stars after big bang with no metals. No mass loss. These stars should exist but they have not been observed.

Pop I stars= stars like our sun with ～2% metal.

Pop II stars= stars with 0.1%～0.01% metal

Pop I and II stars lose their mass in the evolution

From a-LIGO ApJL 818:L22 2016 より

separations). However, if one assumes that the properties of PopIII massive binaries are not very different from binary populations in the local universe (admittedly a considerable extrapolation), then recently predicted BBH total masses agree astonishingly well with GW150914 and can have sufficiently long merger times to occur in the nearby universe (Kinugawa et al. 2014). This is in contrast to the predicted mass properties

Why 30Msun ?

Because it ends its life as blue giant.
While larger mass star ends its life as red giant with large mass loss in the common envelope phase.

Main Sequence
(Hydrogen burning phase)

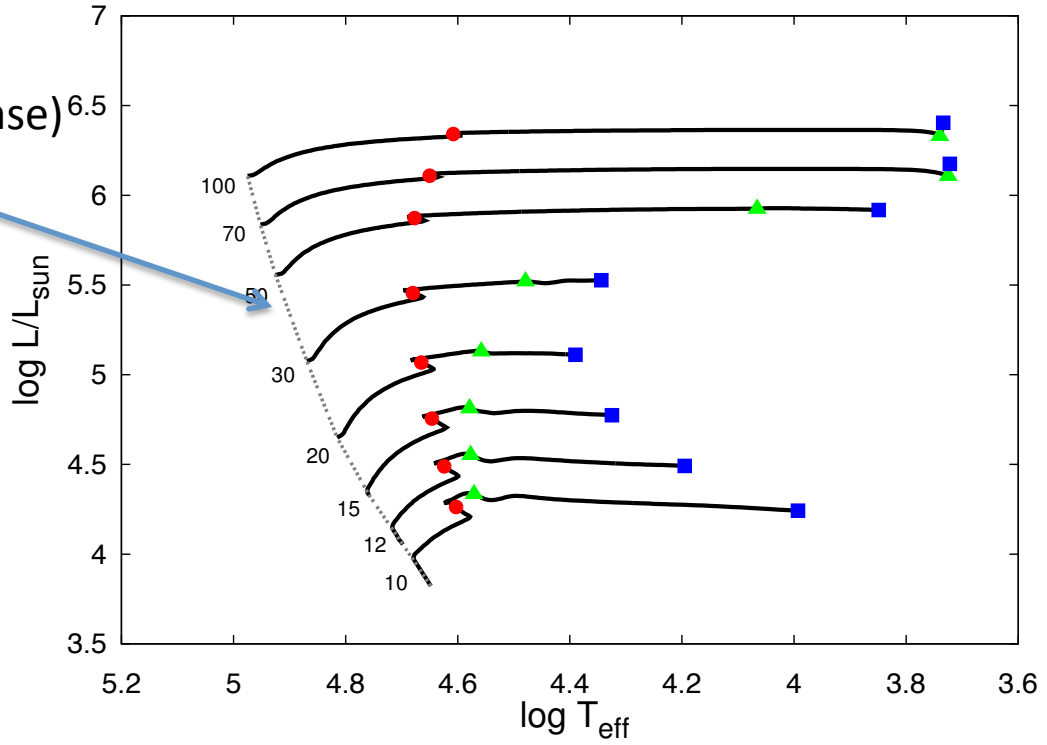

For details,
Kinugawa's talk
on Wednesday.

Figure 1. The Hertzsprung-Russell (HR) diagram for the Pop III stars of mass 10 $M_\odot \leqslant M \leqslant 100\ M_\odot$ using the data taken from Marigo et al. (2001). The number attached to each solid curve is the mass of each star in unit of $M_\odot$. The dashed line shows the ZAMS (Zero Age Main Sequence) stars. Red circles, green triangles and blue squares correspond to the beginning of He-burning, the end of the He-burning and the beginning of the C-burning, respectively.

What is chirp mass?

Consider binary compact stars with mass m_1 and m_2 orbiting circularly with frequency f_{orb}. Then the gravitational wave amplitude h_+ and h_x at distance r is given by

$$h_+=3.2\times10^{-22}(r/200\mathrm{Mpc})^{-1}(M_{chirp}/1.2M_{sun})^{5/6}(f/20\mathrm{Hz})^{-1/6}\cos(2\pi ft)(\cos^2 i+1)/2$$

$$h_x=3.2\times10^{-22}(r/200\mathrm{Mpc})^{-1}(M_{chirp}/1.2M_{sun})^{5/6}(f/20\mathrm{Hz})^{-1/6}\sin(2\pi ft)\cos(i)$$

where $f=2f_{orb}$ and $M_{chirp}=(m_1m_2)^{3/5}/(m_1+m_2)^{1/5}$

i is the inclination angle of the binary.

GW amplitude is in proportion to 5/6 power of chirp mass. Large chirp mass means large GW amplitude!!

My summary talk at GWPAW2016(June) in Boston

- In GWPAW2015(June) Bruce predicted GW150914 using Nakano's presentation and Kinugawa et al.2014
- Now as for chirp mass , BBH >> NS-BH >> NS-NS
- The detectable range is proportional to 5/6 power of the chirp mass and the volume is 5/2
- So that BBH is the easiest detectable source.
- Following this tendency in O2, I predict
- NS-BH will be observed !!
- I hope this slide will be shown first in GWPAW2017 like Bruce's slide in GWPAW2016.

SGRB vs NS-NS and NS-BH

1) Conclusions are

2) As an example if NS-BH is 10% of SGRB, it will be detected in O2 with the rough estimate of events ～ 0.09--4 depending on M_{BH}.

3) NS-NS might have nothing to do with SGRB
or the event rate is higher than expected.

3 important variables of GRBs

- E_{iso}= total energy if the emission is isotropic
- Lp= peak value of the luminosity
- Ep= peak energy of the photon
- for dim GRBs Ep is difficult to determine.
- It is impossible to determine these three values without redshift.
- Are there relations among Ep, Lp and Eiso?
  There are at least two empirical relations.

Yonetoku relation for（Ep-Lp）

- Yonetoku, Murakami, Nakamura et al. in 2004. We only had 11 LGRBs with z, Ep and Lp.

TABLE 1

SPECTRAL PARAMETERS FOR 11 KNOWN-REDSHIFT GRBS OF BATSE

GRB	Redshift	α	β	$E_p(1+z)$ (keV)	Peak Flux (10^{-6} ergs cm^{-2} s^{-1})	Peak Luminosity 10^{52} ergs s^{-1}	χ^2/dof	k_c
970508.....	0.835	$-1.03^{+1.51}_{-0.06}$	$-2.20^{+0.10}_{-0.11}$	$89.8^{+37.8}_{-29.7}$	0.45 ± 0.10	0.14 ± 0.01	43.8/40	1.6
970828.....	0.9578	$-0.45^{+0.06}_{-0.06}$	$-2.06^{+0.08}_{-0.10}$	$742.6^{+29.4}_{-32.1}$	5.93 ± 0.34	3.67 ± 0.15	96.0/82	1.5
971214.....	3.418	$-0.36^{+0.14}_{-0.14}$	$-3.10^{+0.52}_{-6.90}$	$806.7^{+48.6}_{-63.2}$	1.25 ± 0.28	19.51 ± 0.17	68.9/66	1.2
980326.....	0.9–1.1	$-0.93^{+0.09}_{-0.08}$	$-2.96^{+0.21}_{-0.51}$	35.0–100.0	0.65 ± 0.15	0.24–0.40	55.7/48	1.4
980329.....	2.0–3.9	$-0.79^{+0.03}_{-0.03}$	$-2.27^{+0.04}_{-0.05}$	785.0–1085.0	5.79 ± 4.17	12.49–72.38	121.1/112	1.3
980703.....	0.966	$-0.80^{+0.22}_{-0.16}$	$-1.60^{+0.06}_{-0.09}$	>150.0	2.64 ± 0.51	1.76 ± 0.05	89.6/91	1.3
990123.....	1.600	$-0.18^{+0.08}_{-0.07}$	$-2.33^{+0.08}_{-0.09}$	$1333.7^{+49.8}_{-56.9}$	19.6 ± 0.16	31.22 ± 0.23	134.1/112	1.2
990506.....	1.30	$-0.90^{+0.19}_{-0.13}$	$-2.08^{+0.08}_{-0.10}$	$737.6^{+69.2}_{-87.8}$	9.36 ± 0.20	13.28 ± 0.10	108.3/103	1.3
990510.....	1.619	$-0.71^{+0.12}_{-0.12}$	$-3.79^{+0.51}_{-6.21}$	$538.4^{+22.3}_{-32.1}$	2.98 ± 0.18	6.19 ± 0.06	89.9/111	1.4
991216.....	1.020	$-0.66^{+0.04}_{-0.04}$	$-2.44^{+0.12}_{-0.17}$	$1083.7^{+37.3}_{-41.3}$	61.4 ± 1.21	32.36 ± 0.11	125.8/102	1.2
000131.....	4.5	$-0.91^{+0.20}_{-0.15}$	$-2.02^{+0.18}_{-0.32}$	$926.0^{+97.5}_{-83.1}$	2.67 ± 0.41	51.35 ± 7.88	115.1/97	1.4

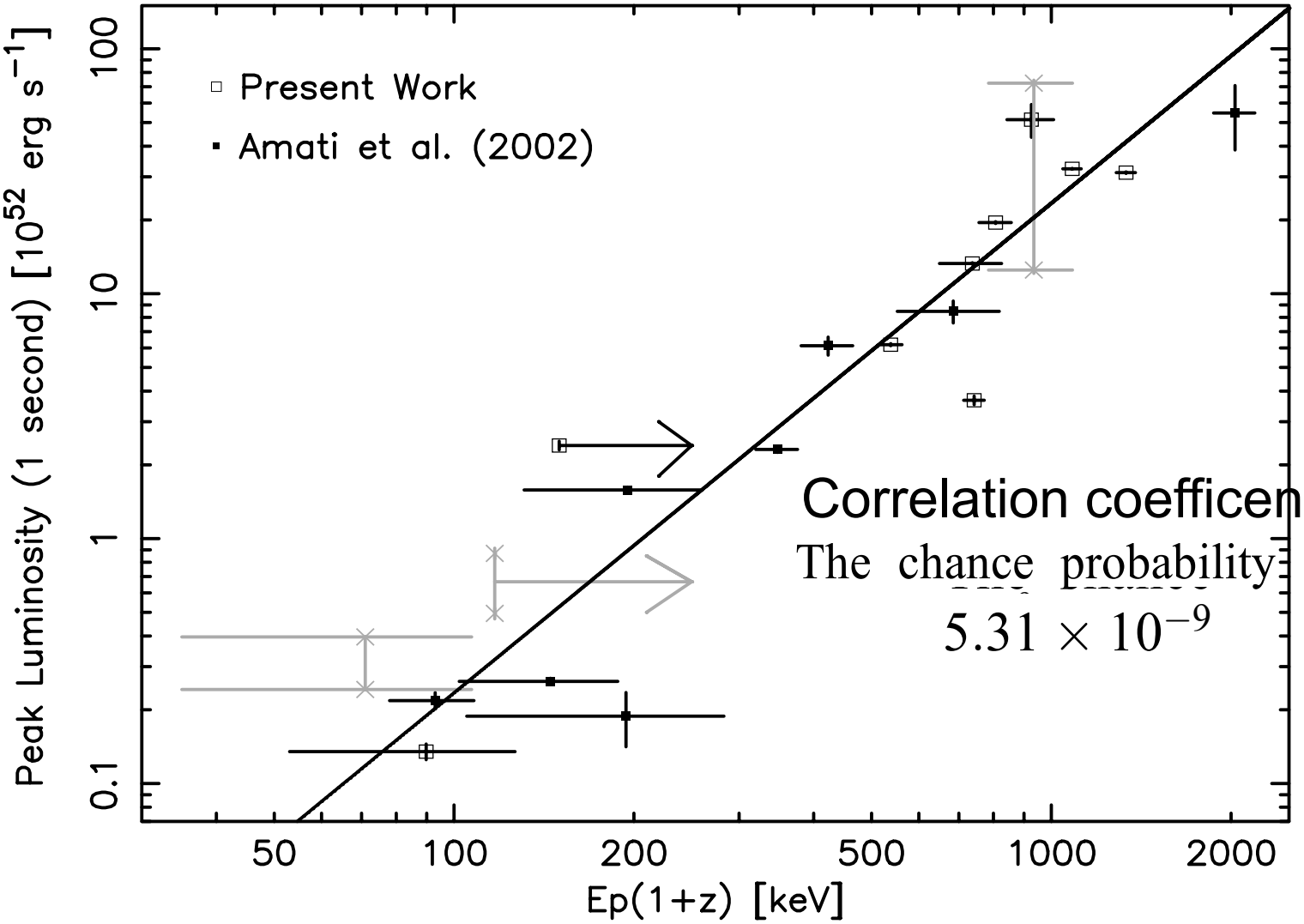

$$\frac{L}{10^{52}\ \mathrm{ergs\ s^{-1}}} = (2.34^{+2.29}_{-1.76}) \times 10^{-5} \left[\frac{E_p(1+z)}{1\ \mathrm{keV}}\right]^{2.0\mp0.2},$$

This relation can be used to determine the redshift of LGRBs.

That is, using the observed flux fp and the peak photon energy Ep with $d_L(z)$ being the luminosity distance to lead $L=4\pi d_L(z)^2 fp$.
Inserting this luminosity into Ep-Lp, only z is unknown.

$$\frac{L}{10^{52}\ \mathrm{ergs\ s^{-1}}} = (2.34^{+2.29}_{-1.76}) \times 10^{-5} \left[\frac{E_p(1+z)}{1\ \mathrm{keV}} \right]^{2.0\mp0.2},$$

Therefore z is determined if you believe in Ep-Lp relation(Yonetoku relation).

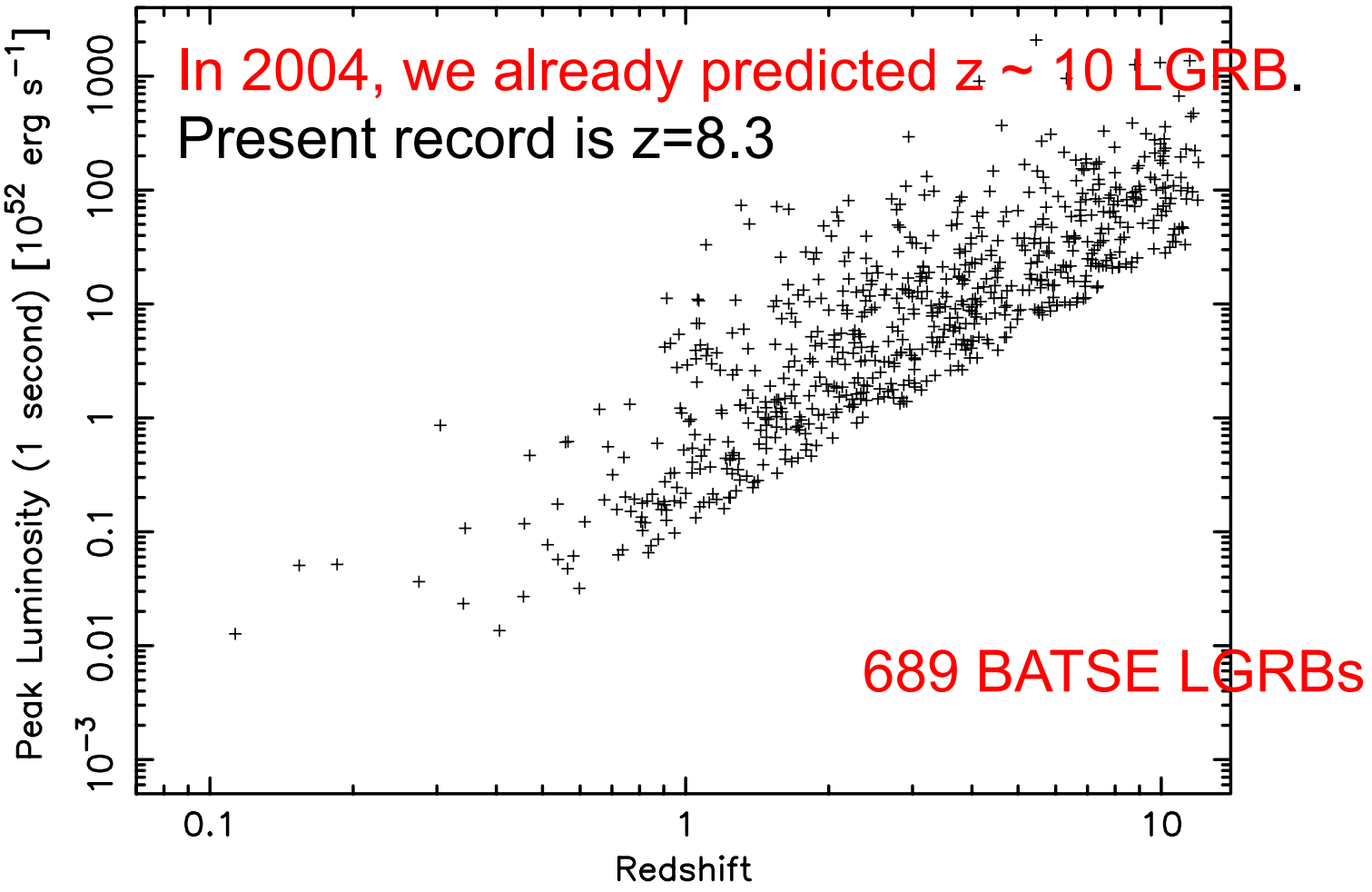

FIG. 2.—Distribution of the peak luminosity vs. redshift derived from the E_p-luminosity relation. The truncation of the lower end of the luminosity is caused by the flux limit of $F_{\rm limit} = 2 \times 10^{-7}$ ergs cm^{-2} s^{-1}.

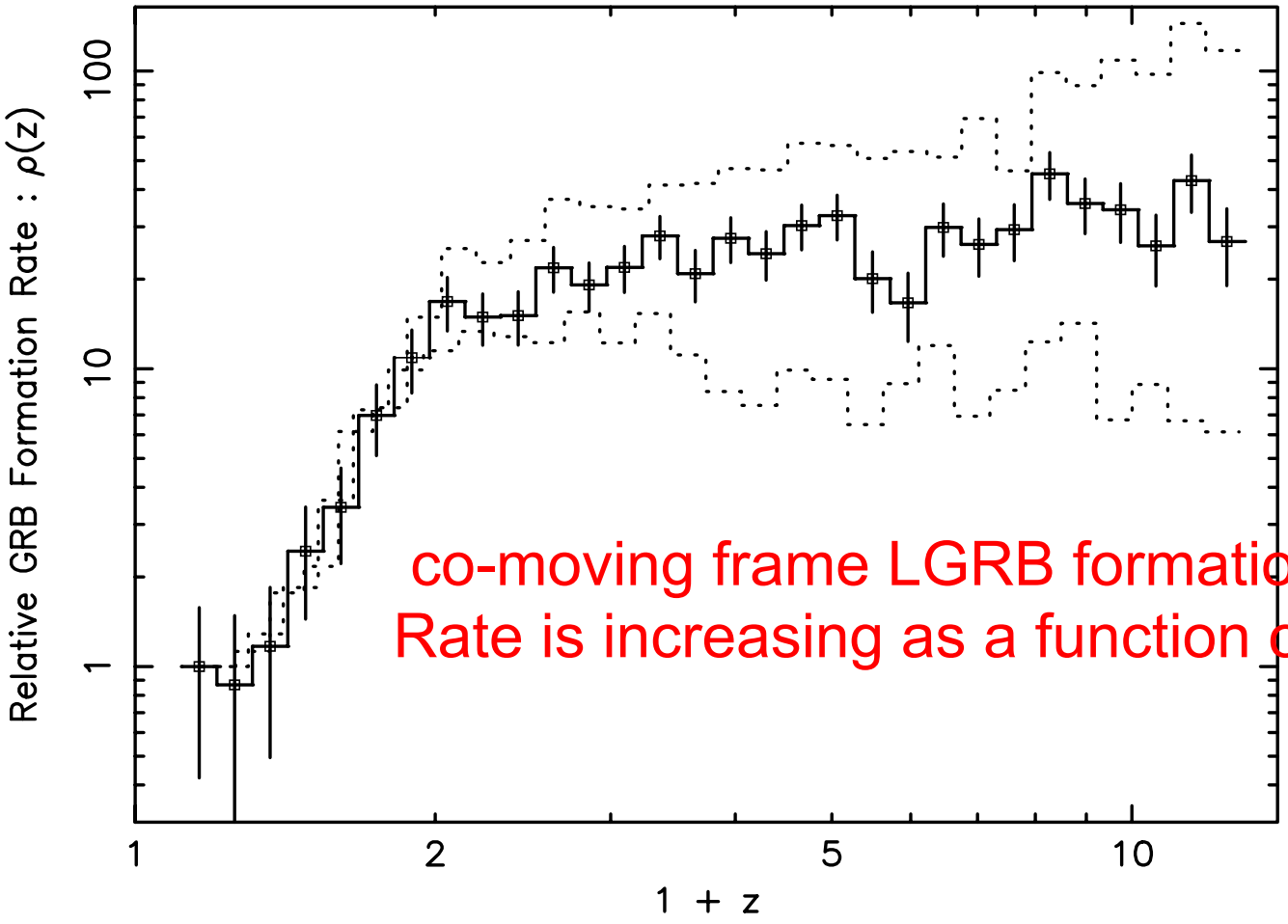

FIG. 8.—Relative GRB formation rate normalized at the first point. The solid line is the result based on the best fit of the E_p-luminosity relation. Two dotted lines indicate the upper and lower bounds caused by the uncertainty of the E_p-luminosity relation, and they are also normalized at the first point. The error bars accompanying the open squares represent the 1 σ statistical uncertainty of each point.

How about Ep-Lp relation for SGRBs？

- Many difficulties existed.
- Since the duration of SGRB is short, the number of photon is small. Therefore the determination of Ep is difficult.
- Many SGRBs have no or dim afterglow, so that it is difficult to determine redshift z.
- As a whole the number of SGRBs with z and Ep has been increasing very slowly.

Tsutsui et al. succeeded to determine Ep--Lp relation in (MNRAS 2013 431, 1398).

13 SGRB candidates. However 5 belong to LGRB. We have only 8 SGRBs.

z, the rest-frame duration $T_{90}^{\rm rest} = T_{90}/(1+z)$, the spectral peak energy $E_{\rm p}$, the peak luminosity $L_{\rm p}$ in 64 ms of the observer frame time bin, the isotropic energy $E_{\rm iso}$, class of SGRB candidates and the reference, respectively. For details see the text.

GRB	Redshift	$T_{90}^{\rm rest}$ (s)	$E_{\rm p}$ (keV)	$L_{\rm p}$ (erg s^{-1})	$E_{\rm iso}$ (erg)	Class	Ref.[a]
040924	0.86	0.81	$124.55^{+11.15}_{-11.15}$	$(2.28^{+0.25}_{-0.24}) \times 10^{52}$	$(1.01^{+0.05}_{-0.05}) \times 10^{52}$	Misguided	(1)
050709[b]	0.16	0.60	$97.32^{+7.76}_{-0.58}$	$(7.51^{+0.76}_{-0.81}) \times 10^{50}$	$(4.33^{+0.29}_{-0.30}) \times 10^{49}$	Secure	(2)
051221	0.55	0.91	$621.69^{+87.42}_{-67.69}$	$(2.77^{+0.29}_{-0.29}) \times 10^{52}$	$(3.53^{+0.43}_{0.31}) \times 10^{51}$	Secure	(3)
061006	0.44	0.35	$954.63^{+198.39}_{-125.86}$	$(2.06^{+0.15}_{-0.31}) \times 10^{52}$	$(9.83^{+0.20}_{-0.94}) \times 10^{51}$	Secure	(4)
070714B	0.92	1.04	$2150.40^{+910.39}_{-443.52}$	$(6.56^{+0.79}_{-1.36}) \times 10^{52}$	$(1.61^{+0.18}_{-0.24}) \times 10^{52}$	Secure	(5)
071020	2.15	1.11	$1012.69^{+152.94}_{-101.33}$	$(3.06^{+0.35}_{-1.04}) \times 10^{53}$	$(1.24^{+0.04}_{-0.47}) \times 10^{53}$	Misguided	(6)
080913	6.70	1.04	$1008.05^{+1052.52}_{-224.54}$	$(3.18^{+0.28}_{-0.50}) \times 10^{53}$	$(1.09^{+0.11}_{-0.08}) \times 10^{53}$	Misguided	(7)
090423	8.26	1.30	$612.36^{+193.53}_{-193.53}$	$(4.63^{+9.95}_{-1.48}) \times 10^{53}$	$(1.17^{+1.45}_{-0.38}) \times 10^{53}$	Misguided	(8)
090510	0.90	0.16	$8679.58^{+947.69}_{-947.69}$	$(1.04^{+0.24}_{-0.14}) \times 10^{54}$	$(4.54^{+1.05}_{-0.61}) \times 10^{52}$	Secure	(8)
100117A	0.92	0.16	$936.96^{+297.60}_{-297.60}$	$(1.89^{+0.21}_{-0.35}) \times 10^{52}$	$(1.87^{+0.23}_{-0.23}) \times 10^{51}$	Secure	(8)
100206	0.41	0.09	$638.98^{+131.21}_{-131.21}$	$(9.98^{+11.50}_{-3.25}) \times 10^{51}$	$(7.63^{+7.89}_{-2.29}) \times 10^{50}$	Secure	(8)
100816A	0.81	1.11	$235.36^{+15.74}_{-15.74}$	$(9.69^{+1.95}_{-1.28}) \times 10^{51}$	$(9.03^{+1.52}_{-1.04}) \times 10^{51}$	Misguided	(8)
101219A	0.72	0.35	$841.82^{+107.56}_{-82.50}$	$(1.56^{+0.24}_{-0.23}) \times 10^{52}$	$(8.81^{+1.00}_{-1.05}) \times 10^{51}$	Secure	(9)

[a]References for spectral parameters, peak fluxes and fluences: (1) Golenetskii et al. (2004); (2) Villasenor et al. (2005); (3) Golenetskii et al. (2005); Norris et al. (2005); (4) Golenetskii et al. (2006); (5) Ohno et al. (2007); Kodaka et al. (2007); (6)

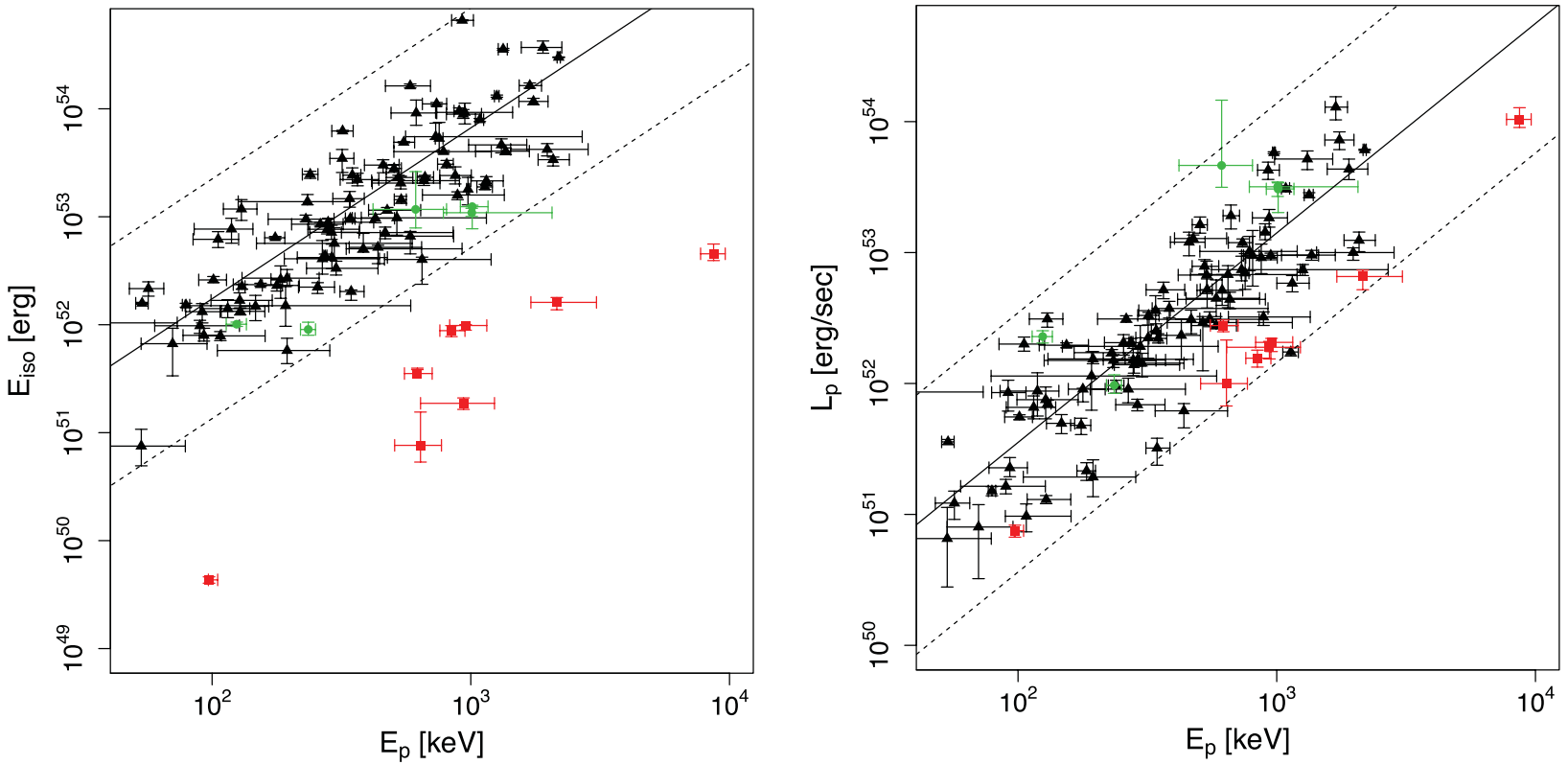

Figure 1. The E_p–E_{iso} (left) and E_p–L_p (right) diagrams. The LGRBs from Yonetoku et al. (2010) are marked with the black filled triangles, misguided SGRBs with the green filled circles and secure SGRBs with the red filled squares. The best-fitting function and $3\sigma_{int}$ dispersion of the correlations of LGRBs from Yonetoku et al. (2010) are indicated with the black solid and dotted lines, respectively. The peak luminosities of LGRBs are defined by 1024 ms bin in the observer frame, while those of SGRBs by 64 ms bin in the observer frame.

Left Ep-Eiso relation(Amati relation)
Black triangles→ LGRBs
Green → not SGRB but LGRB
Red squares → Secure SGRB

Right Ep-Lp(Yonetoku relation)
black solid line → Ep-Lp for LGRBs with 3σ dotted lines
All secure SGRBs are below Black solid line

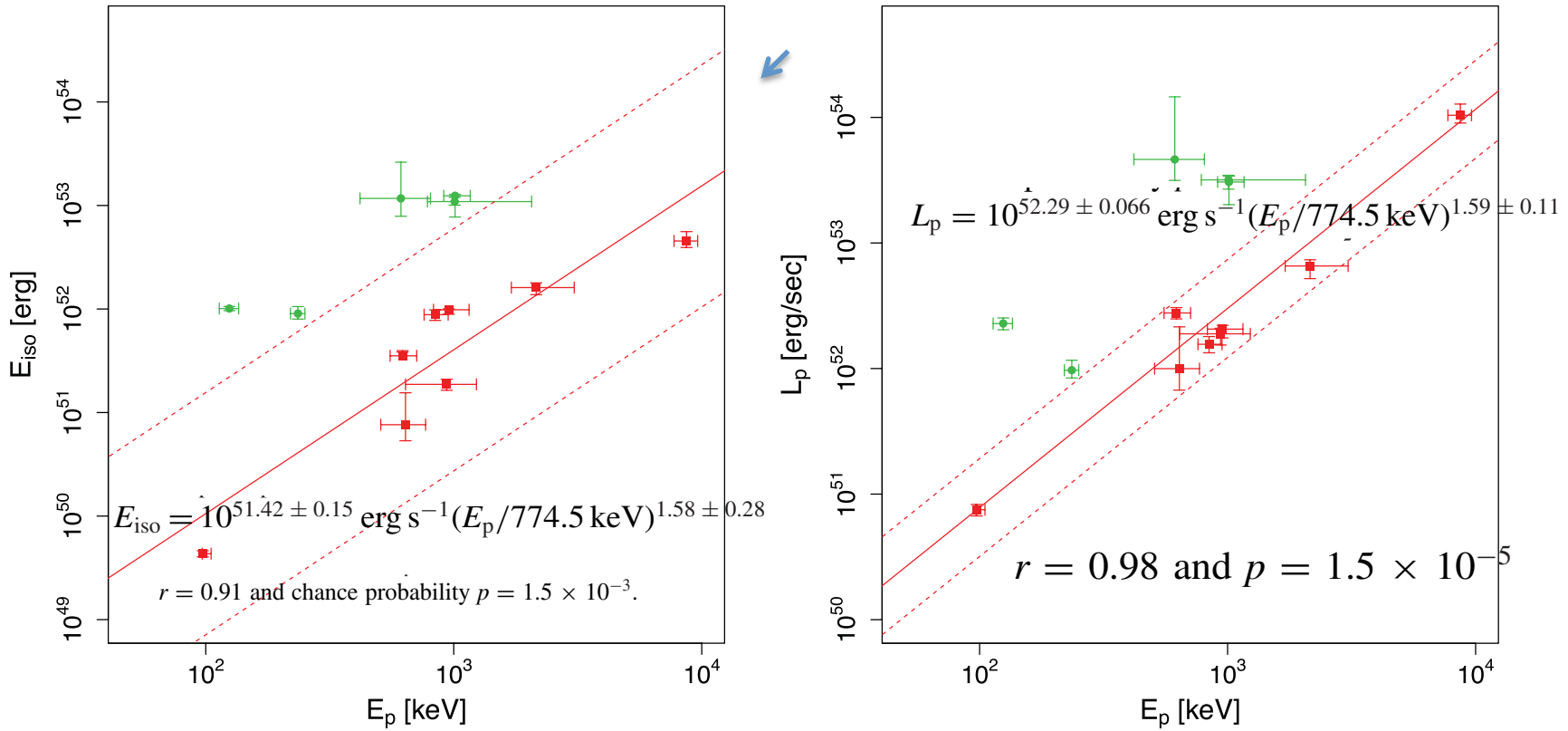

Figure 2. Left: the $E_p - E_{iso}$ diagram for SGRBs. Right: the $E_p - L_p$ diagram for SGRBs. In each figure, misguided SGRBs are marked with green filled circles, and secure SGRBs with red filled squares. The best-fitting function and $3\sigma_{int}$ dispersion are indicated with the red solid and dotted lines, respectively.

Left
Ep-Eiso relation for SGRB
is 100 times dimmer than that
of LGRB

Right
Ep-Lp relation for SGRB
is 5 times dimmer than that
of LGRB

BATSE Bright SGRB Ghirlanda, Nava Ghisellini at al. 2009 with no z information

Table 6. The sample of 79 short BATSE GRBs.

Trig.	T_{90} s	P phot/(cm^2 s)	α	E_0 keV	χ^2(dof)	Fluence erg/cm^2	Peak flux erg/(cm^{2}s)
6293	0.192±0.091	88.53±1.00	-1.27±0.02		1.216(109)	4.56E-6	>5.74E-5
298	0.455±0.065	56.13±1.27	-0.57±0.92	85.38± 64.90	1.113(102)	1.99E-7	1.43E-5
3412	0.068±0.006	54.82±0.76	-1.31±0.52	110.20± 80.98	0.892(103)	2.62E-7	1.91E-5
6668	0.116±0.006	39.12±0.61	-0.39±0.49	126.80± 62.57	1.184(107)	4.99E-7	1.18E-5
444	0.256±0.091	28.55±0.76	-0.87±0.23	113.50± 28.39	1.132(102)	5.07E-7	8.04E-6
2514	0.200±0.094	28.40±0.74	-0.81±0.14	163.30± 25.95	1.129(100)	1.12E-6	8.99E-6
3152	1.793±0.066	25.34±0.72	-0.40±0.09	683.70±116.50	1.175(107)	6.55E-6	4.64E-5
5561	0.104±0.011	19.28±0.45	-1.20±1.48	48.51± 25.00	0.956(108)	1.65E-7	8.69E-6
3087	1.152±0.091	18.68±0.58	-1.19±0.15	273.10± 74.50	1.103(76)	2.89E-6	7.02E-6
2273	0.224±0.066	18.59±0.55	-0.18±0.45	132.70± 49.46	0.886(100)	3.88E-7	6.26E-6
7281	1.664±0.143	16.83±0.42	-0.83±0.15	123.30± 18.60	1.296(107)	2.21E-6	4.80E-6
2068	0.591±0.060	15.63±0.59	-0.22±0.26	97.07± 22.85	1.210(107)	3.91E-7	4.19E-6
2125	0.223±0.013	15.42±0.56	-0.48±0.30	240.50± 90.00	0.844(102)	4.57E-7	7.43E-6
3173	0.208±0.025	14.90±0.58	-1.00±0.18	559.60±281.65	1.356(105)	6.69E-7	9.52E-6
2679	0.256±0.091	13.73±0.51	-0.32±0.13	650.20±149.25	1.363(107)	3.14E-6	2.72E-5
1553	0.960±0.143	13.70±0.52	-0.87±0.11	764.00±183.60	1.173(96)	6.62E-6	1.35E-5
6123	0.186±0.042	12.83±0.42	-0.23±1.64	76.66± 49.00	1.107(108)	1.11E-7	3.10E-6
6635	1.152±0.143	12.05±0.39	-1.74±0.15	129.50± 32.70	1.014(91)	2.76E-6	6.57E-6
1088	0.192±0.091	11.92±0.55	0.10±2.11	68.08± 61.79	1.186(104)	7.41E-8	2.80E-6
1453	0.192±0.453	11.89±0.51	-0.16±0.65	94.20± 48.00	0.812(108)	1.80E-7	3.17E-6
6535	1.664±0.143	11.88±0.38	-0.97±0.08	1175.60±384.27	1.391(108)	7.36E-6	1.47E-5
2320	0.608±0.041	11.03±0.47	-0.58±0.19	129.00± 26.10	0.794(103)	7.57E-7	3.23E-6
2933	0.320±0.091	10.77±0.44	0.22±0.62	130.20± 55.94	1.429(107)	3.42E-6	4.33E-6
7939	1.039±0.072	10.77±0.38	-0.41±0.15	99.73± 12.96	1.193(82)	2.53E-6	2.86E-6
2614	0.296±0.057	10.49±0.52	-1.00±0.18	469.60±222.80	0.836(108)	6.08E-7	5.84E-6
2715	0.384±0.091	10.47±0.50	0.08±0.11	562.80± 85.20	1.049(108)	7.69E-6	3.30E-5
2896	0.456±0.033	10.44±0.48	-0.87±0.26	79.94± 18.19	1.072(106)	7.53E-7	2.89E-6
7784	1.918±1.995	10.29±0.34	-0.83±0.35	140.20± 54.30	1.432(108)	5.63E-7	3.05E-6
2317	0.896±0.091	9.73±0.46	-0.53±0.25	73.46± 13.12	1.249(65)	1.04E-6	2.41E-6
2834	0.680±0.011	8.79±0.44	-0.54±0.24	407.60±168.80	1.165(85)	1.36E-6	6.90E-6
6679	1.408±0.091	8.62±0.35	-0.61±0.27	318.90±141.60	1.409(107)	9.39E-7	4.91E-6
6527	1.856±0.516	8.47±0.38	-1.32±0.21	80.36± 15.60	1.090(95)	3.33E-6	3.25E-6
7353	0.249±0.004	8.47±0.38	0.00±0.22	615.80±197.40	1.181(107)	4.19E-6	2.72E-5
5277	0.496±0.023	8.14±0.33	0.29±0.24	208.40± 30.81	0.885(106)	1.54E-6	6.46E-6
8104	0.384±0.091	8.13±0.30	0.42±1.35	110.60± 70.37	0.774(107)	2.20E-7	3.04E-6
2330	0.804±0.009	8.03±0.39	-0.86±0.29	616.90±491.30	0.961(75)	1.02E-6	6.54E-6
6263	1.984±0.181	7.99±0.31	-0.36±0.64	69.14± 30.59	1.054(107)	3.78E-7	1.91E-6
5339	0.832±0.091	7.77±0.33	-0.40±0.10	567.90± 99.64	0.732(93)	4.95E-6	1.12E-5
603	1.472±0.272	7.50±0.56	-0.71±0.63	155.30± 93.62	1.004(85)	3.78E-7	2.36E-6
6368	0.896±0.326	7.24±0.34	-1.37±0.18		0.997(108)	3.21E-7	>4.26E-6
6606	0.704±0.389	7.16±0.29	-1.77±0.20		0.973(108)	5.02E-7	>3.04E-6
3642	0.704±0.091	6.83±0.31	0.21±0.88	89.97± 58.42	1.262(107)	2.92E-7	1.93E-6
6671	0.256±0.091	6.71±0.31	-1.39±0.13		0.937(100)	5.36E-7	>3.84E-6
5647	1.088±0.326	6.50±0.32	-0.06±0.80	108.50±115.16	1.366(107)	1.74E-7	1.95E-6
7375	0.311±0.073	6.40±0.31	-0.47±0.87	267.90±200.05	1.039(101)	3.19E-7	3.46E-6
677	0.055±0.008	6.21±0.44	0.65±1.29	127.20±168.26	0.751(105)	1.22E-7	3.18E-6
1076	0.161±0.016	6.18±0.44	-2.46±0.33		1.417(89)	1.20E-7	>2.16E-6
936	1.438±0.065	5.85±0.44	-0.84±0.26	341.50±179.45	1.069(104)	7.03E-7	2.91E-6
5607	1.088±0.091	5.85±0.30	-0.71±0.23	426.20±199.45	1.150(82)	1.19E-6	3.97E-6
7142	0.969±0.064	5.81±0.28	0.94±0.33	124.10± 12.79	0.953(107)	1.42E-6	3.50E-6
4955	0.464±0.036	5.73±0.31	-1.04±0.45	298.20±371.80	1.176(107)	2.71E-7	2.33E-6
4776	0.448±0.091	5.54±0.28	-0.19±0.32	232.70± 88.45	1.152(107)	6.90E-8	3.27E-6
7813	0.564±0.164	5.37±0.29	-2.68±0.17		1.053(108)	5.59E-7	>1.94E-6
1760	0.576±0.143	5.27±0.35	-0.25±0.28	188.70± 56.95	1.027(105)	6.18E-7	2.37E-6
7378	1.247±0.077	5.25±0.33	-0.52±0.16	536.20±153.35	1.465(107)	2.60E-6	5.87E-6
4660	1.168±0.080	5.15±0.29	0.56±0.21	161.70± 23.80	0.919(87)	1.92E-6	3.53E-6
5533	0.768±0.091	5.12±0.30	0.02±0.15	335.20± 60.15	0.971(87)	2.91E-7	6.26E-6
7078	0.448±0.091	5.11±0.42	-3.60±0.45		0.920(108)	1.73E-7	>2.90E-6

Table 6. continue....

Trig.	T_{90} s	P phot/(cm^2 s)	α	E_0 keV	χ^2(dof)	Fluence erg/cm^2	Peak flux erg/(cm^{2}s)
5527	0.820±0.008	5.04±0.26	-0.34±0.11	489.30± 88.30	0.760(90)	3.73E-6	6.41E-6
3735	1.301±0.091	4.83±0.29	0.00±0.18	301.70± 55.05	1.286(107)	2.60E-6	4.91E-6
3297	0.272±0.023	4.45±0.33	-0.83±0.37	496.80±501.70	1.198(106)	4.90E-7	3.07E-6
2952	0.680±0.018	4.37±0.34	-0.69±0.25	570.20±312.15	0.791(107)	8.76E-7	4.13E-6
5599	0.598±0.043	4.24±0.26	-0.79±0.30	664.70±637.40	1.234(106)	8.25E-7	4.07E-6
5529	1.015±0.129	4.23±0.29	1.37±0.96	65.65± 22.09	1.015(106)	2.95E-7	1.31E-6
7133	1.079±0.37	4.08±0.26	-0.14±0.29	135.80± 36.25	1.115(107)	6.01E-7	1.43E-6
7793	1.093±0.04	3.99±0.27	-0.05±0.22	470.90±126.35	1.054(106)	4.34E-6	7.56E-6
2377	0.496±0.011	3.98±0.33	0.06±0.26	229.30± 55.10	0.875(100)	6.90E-7	2.91E-6
3606	1.824±0.066	3.95±0.26	0.19±0.35	175.90± 49.60	1.216(102)	1.72E-6	2.26E-6
3113	0.976±0.023	3.90±0.35	-0.78±0.16	690.00±316.25	1.145(90)	1.54E-6	3.95E-6
6715	0.452±0.027	3.71±0.26	-0.25±0.78	206.20±187.77	1.178(107)	4.34E-7	1.83E-6
575	0.413±0.022	3.70±0.46	0.17±0.87	121.40± 63.56	0.890(106)	1.71E-7	1.35E-6
2217	0.656±0.029	3.56±0.31	0.36±0.27	281.00± 93.35	1.234(73)	1.46E-6	4.97E-6
3921	0.464±0.161	3.52±0.24	0.36±0.48	179.90± 66.60	1.086(106)	5.42E-7	2.39E-6
5206	0.304±0.023	3.46±0.28	-1.23±0.09		1.219(107)	3.81E-7	>2.34E-6
2918	0.448±0.091	3.44±0.34	-0.60±0.63	252.50±195.90	1.085(100)	1.77E-7	1.59E-6
3940	0.576±0.091	3.19±0.22	-0.33±0.44	101.80± 40.67	1.187(97)	2.50E-7	8.64E-7
7912	1.856±0.707	3.10±0.25	-0.28±0.26	150.90± 47.65	1.236(107)	8.05E-7	1.11E-6
6341	1.920±0.707	3.05±0.28	-0.25±0.29	332.00±143.20	0.878(107)	1.34E-6	2.64E-6
3359	0.344±0.025	3.01±0.25	0.67±0.90	121.00± 74.79	1.037(104)	2.35E-7	1.46E-6

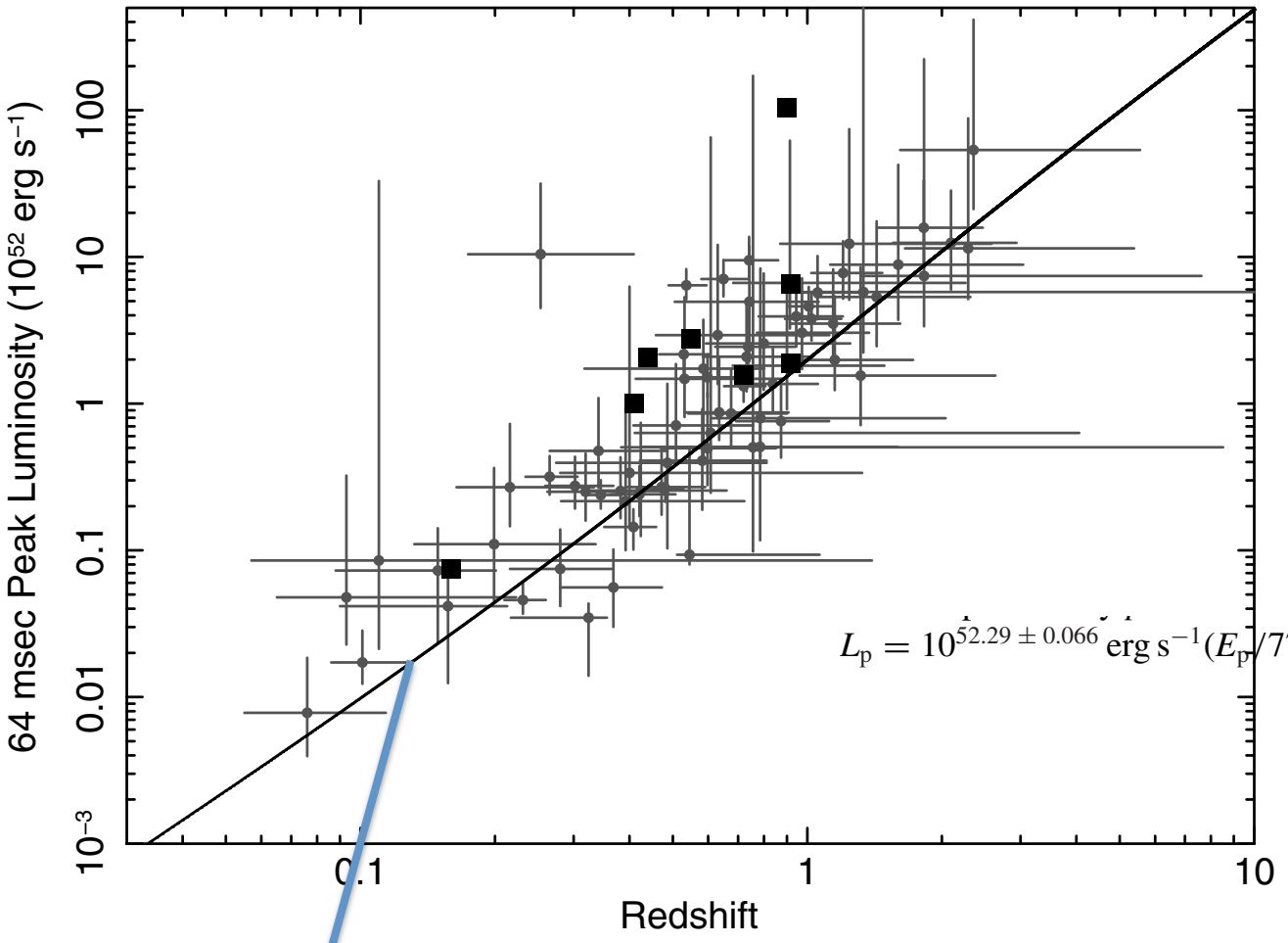

Yonetoku, et al. MNRAS 789 (2014)

Figure 1. Redshift distribution of SGRBs estimated by the E_p–luminosity correlation by Tsutsui et al. (2013). The solid squares are the known redshift samples, and the solid circles are those of pseudo-redshifts. The solid line is the flux limit of 4×10^{-6} erg cm^{-2} s^{-1}.

72 bright BATSE SGRBs with Ep. Using Ep-Lp relation of SGRB we determined z.
To derive the luminosity function and the event rate we used 45 SGRBs above the solid line of fp= 4x10^{-6}erg cm^{-2} s^{-1} so that we determined the lower limit of the event rate.
Squares are 8 SGRBs to determine Ep-Lp relation for SGRB.

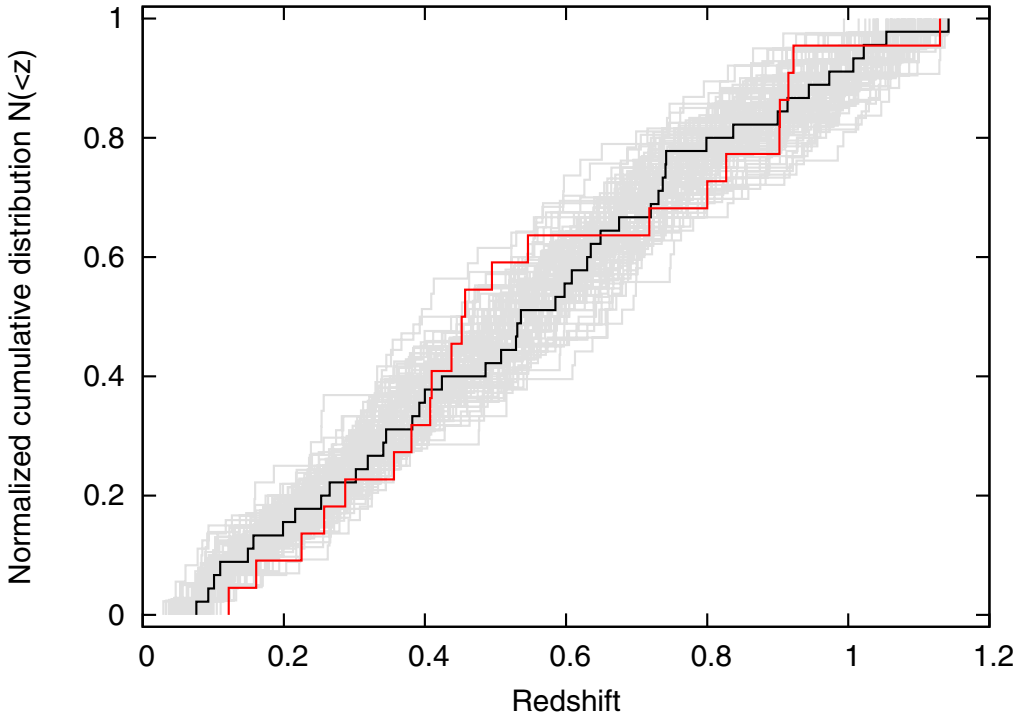

Figure 3. Cumulative redshift distribution of SGRBs up to $z = 1.14$. The black and the red solid lines are for 45 BATSE SGRBs in this paper and 22 known redshift samples observed by HETE-2 and *Swift*/BAT, respectively. The gray solid lines behind them show possible error regions estimated by the 100 Monte Carlo simulations. We can see the good agreement of red, black, and gray lines in the entire region. The Kolmogorv–Smirnov test between the black and red lines shows that the probability that the two curves arise from different distribution is 79.4%, and the error region shown in gray lines covers the red line. This strongly suggests that the E_p–L_p correlation for SGRB (Tsutsui et al. 2013) is a good distance indicator.

Black lines : cumulative redshift distribution of 45 BATSE SGRBs

Red lines : cumulative redshift distribution of 22 SGRBs by HETE-2 and Swift.

Grey : 100 Mont Carlo Simulations taking into Account of error in Ep and Lp

The list of SGRBs with the observed or limit of z Fong, Bergers and Chornock et al. 2013

Table 1
Short GRB Host Galaxy Morphologies

GRB	T_{90}[a] (s)	z[b]	Type[c]	90% XRT Uncert.[d] (arcsec)	$P_{cc}(<\delta R)$	References
			Subarcsecond localized			
050709	0.07/130	0.161	L		3×10^{-3}	1–3
050724A	3	0.257	E		2×10^{-5}	4–5
051221A	1.4	0.546	L		5×10^{-5}	6–7
060121	2.0	<4.1	?		2×10^{-3}	8–9
060313	0.7	<1.7	?		3×10^{-3}	10–11
061006	0.4/130	0.4377	L		4×10^{-4}	12–15
061201	0.8	0.111	H/L		··· /0.08	9, 16–17
070429B	0.5	0.9023	L		3×10^{-3}	18–19
070707	1.1	<3.6	?		7×10^{-3}	20–21
070714B	2.0/64	0.9224	L		5×10^{-3}	19, 22–23
070724A	0.4	0.457	L		8×10^{-4}	24–25
070809	1.3	0.473	H/E		··· /0.03	9, 26
071227	1.8[e]	0.381	L		0.01	27–29
080503	0.3/170	<4.2	H/?		··· /0.1	9, 30–31
080905A	1.0	0.1218	L		0.01	32–33
081226A	0.4	<4.1	?		0.01	34–35
090305	0.4	<4.1	H/?		··· /0.06	9, 36
090426A	1.3	2.609	L		1.5×10^{-4}	37–38
090510	0.3	0.903	L		8×10^{-3}	39–40
090515	0.04	0.403	H/E		··· /0.15	9, 41
091109B	0.3	<4.4	?		...	42–43
100117A	0.3	0.915	E		7×10^{-5}	44–45
110112A	0.5	<5.3	H/?		0.43	46, This work
111020A[f]	0.4	...	?		0.01	47–48
111117A[f g]	0.5	1.3	L		0.02	49–50
			XRT only			
050509B	0.04	0.225	E	3.8	5×10^{-3}	51–52
050813[h]	0.6	0.72/1.8	E/?	2.9	...	53–57
051210	1.3	>1.4	?	1.6	0.04	14, 58
060502B	0.09	0.287	E	5.2	0.03	59–60
060801	0.5	1.130	L	1.5	0.02	61–62
061210	0.2/85	0.4095	L	3.9	0.02	14, 63
061217	0.2	0.827	L	5.5	0.24[i]	14, 64
070729[g]	0.9	0.8	E	2.5	0.05	65–66
080123	0.4/115	0.495	L	1.7	0.004	67–68
100206A	0.1	0.4075	L	3.3	0.02	69–70
100625A	0.3	0.452	E	1.8	0.04	71, This work
101219A	0.6	0.718	L	1.7	0.06	72, This work

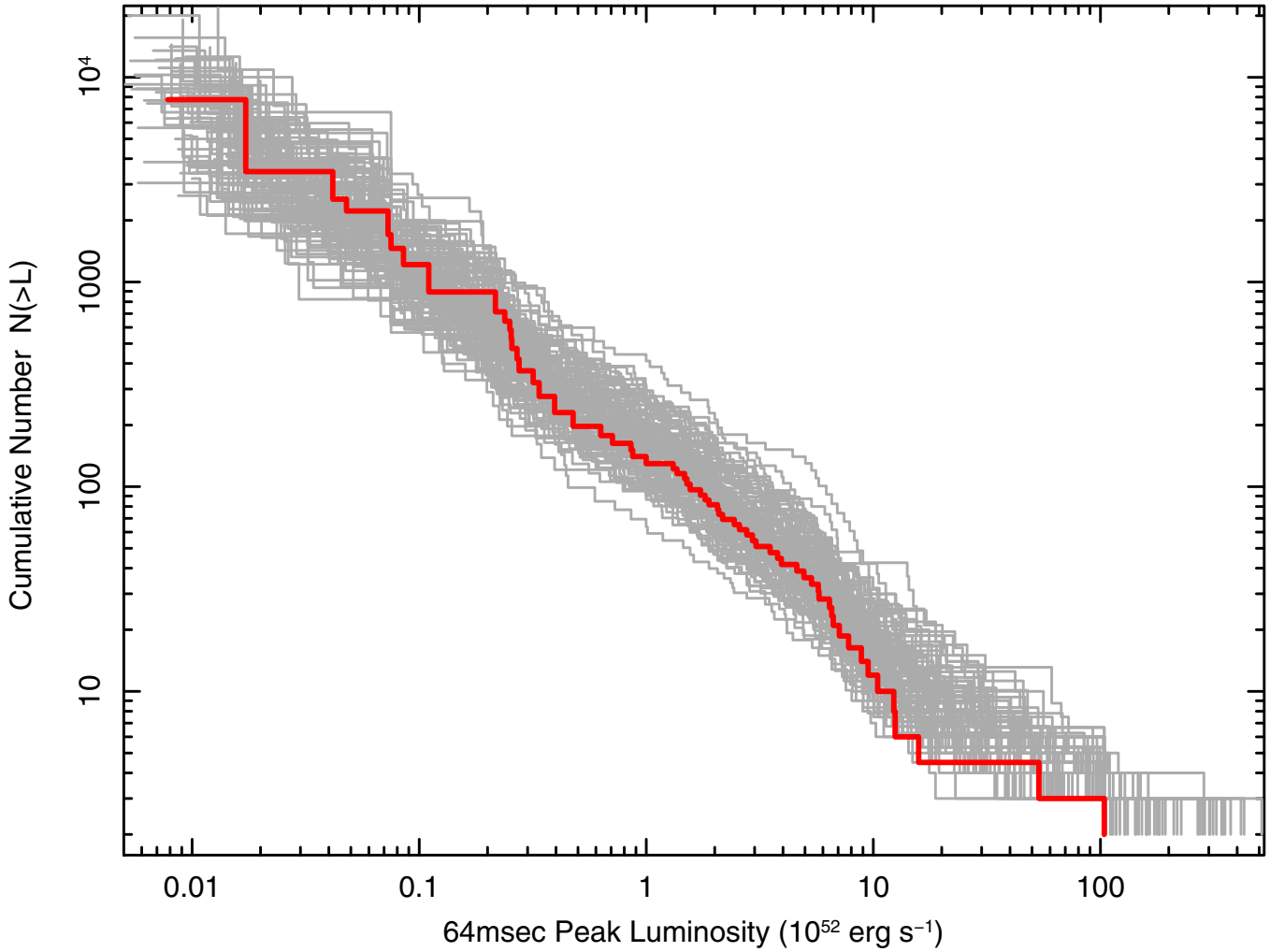

Red line : the cumulative luminosity function $\propto L^{-1}$

Grey lines: 100 Mont Carlo simulations

Figure 4. Luminosity function of SGRBs estimated from the data distribution of Figure 1. The red solid line shows one of the best estimations, and the 100 gray lines are the possible error region estimated by the Monte Carlo simulations. We can approximately describe it as a simple power-law function with an index of -1, and no obvious break has been found.

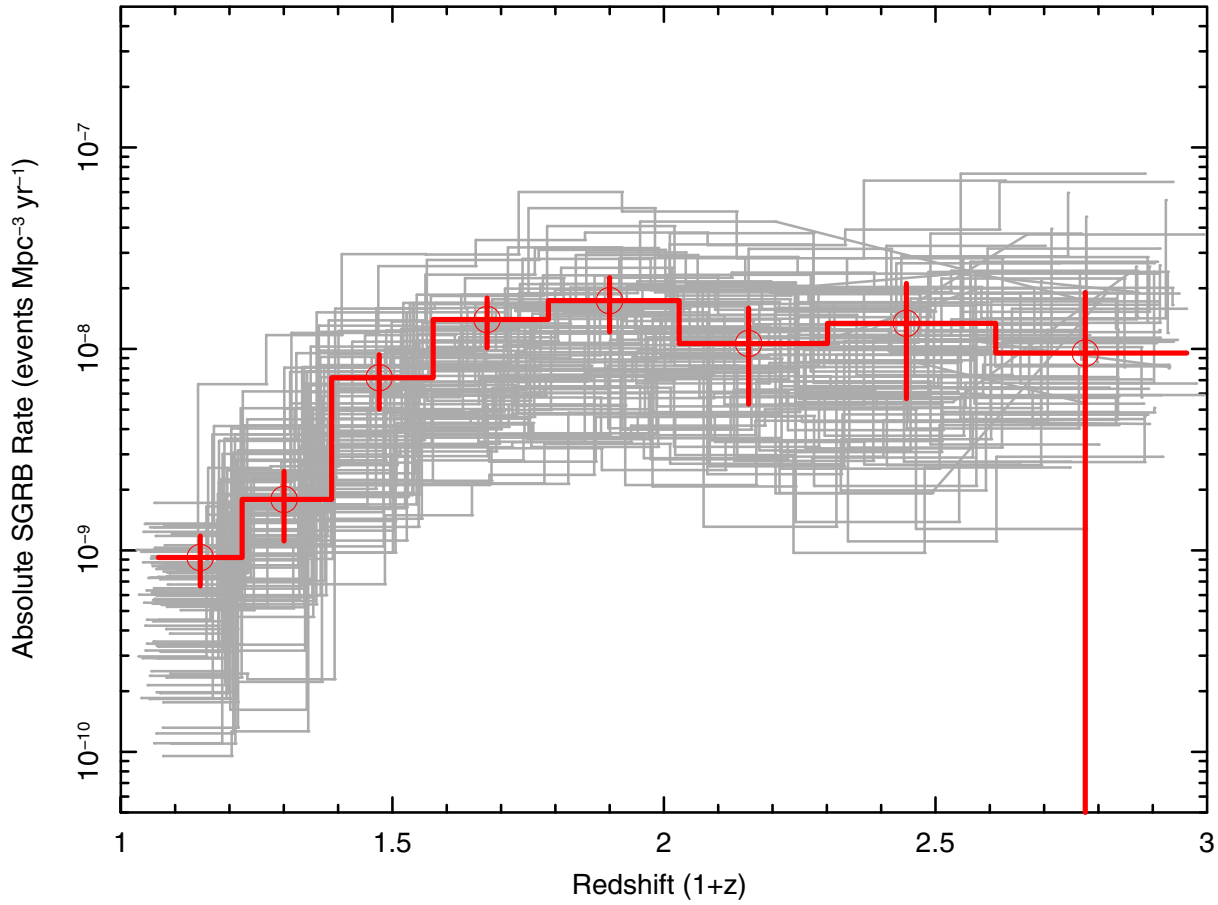

Figure 5. Absolute formation rate of SGRBs estimated from the data distribution of Figure 1. Again, the red line is the best estimation and the 100 gray lines are those from Monte Carlo simulations. The local event rate at $z = 0$ is $\rho_{\rm SGRB}(0) = 6.3^{+3.1}_{-3.9} \times 10^{-10}\,{\rm events\,Mpc^{-3}\,yr^{-1}}$.

Red line:
SGRB formation rate

Grey lines: 100 Mont Carlo simulations.

As an example, assuming 10% of SGRB is NS-BH and a factor 4 dim SGRB with beaming factor 100,
rough estimate of events in O2 are .

NS-BH mass	range(Mpc)	expected events in O2
1.4-5Msun	～160	0.09-0.35
1.4-10Msun	～210	0.19-0.74
1.4-20Msun	～270	0.49- 1.9
1.4-30Msun	～370	1.00- 4.0
1.4-1.4Msun	～100	0.2-0.79 (All SGRB=NS-NS)

Possible X ray Emission

Wide Extended and Plateau emission?

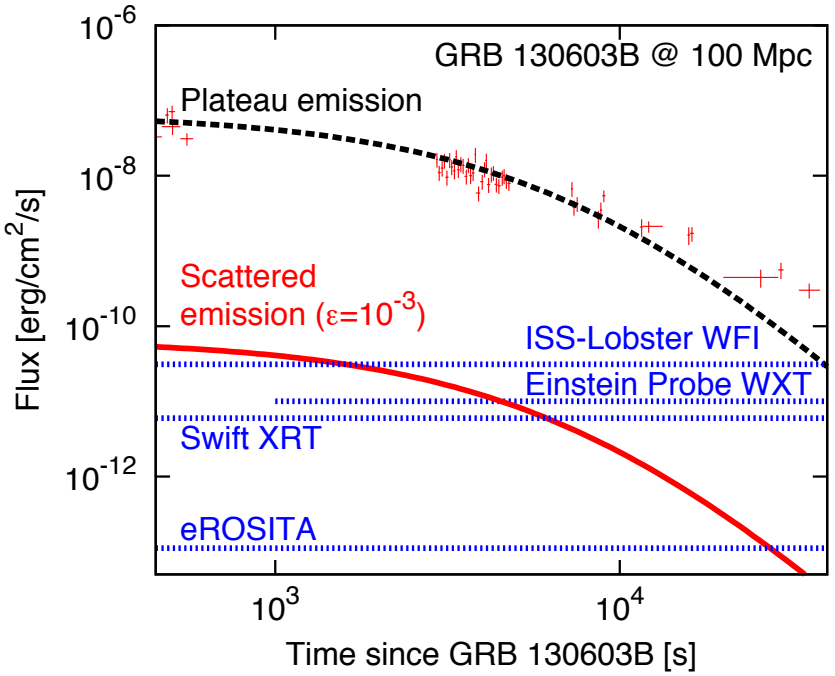

FIG. 2.— Light curves of the plateau (the black dashed curve) and its scattered emissions ($\epsilon = 10^{-3}$; the red solid curve). Red crosses are the plateau emission of GRB 130603B with the distance changed from the original redshift $z = 0.356$ to 100 Mpc. Observational data are obtained from UK *Swift* Science Data Centre. Blue dotted lines show the sensitivity limits for the soft X-ray detectors of *ISS-Lobster*/WTI (integration time 450 s), *Einstein Probe*/WXT (integration time 1000 s), *Swift*/XRT (integration time 100 s) and *eROSITA* (integration time corresponding to a single survey pass). The scattered emission is detectable for these X-ray detectors.

Polarization degree is

$$\Pi = (1-\cos^2\theta)/(1+\cos^2\theta)$$

Scattered X-ray is polarized.

θ is the inclination angle of the binary.

Direction of the polarization is the same as the Ascending node

These two values can be determined by GW also.

Kisaka, Ioka & Nakamura 2015

Scattered X- ray can be seen from every direction.

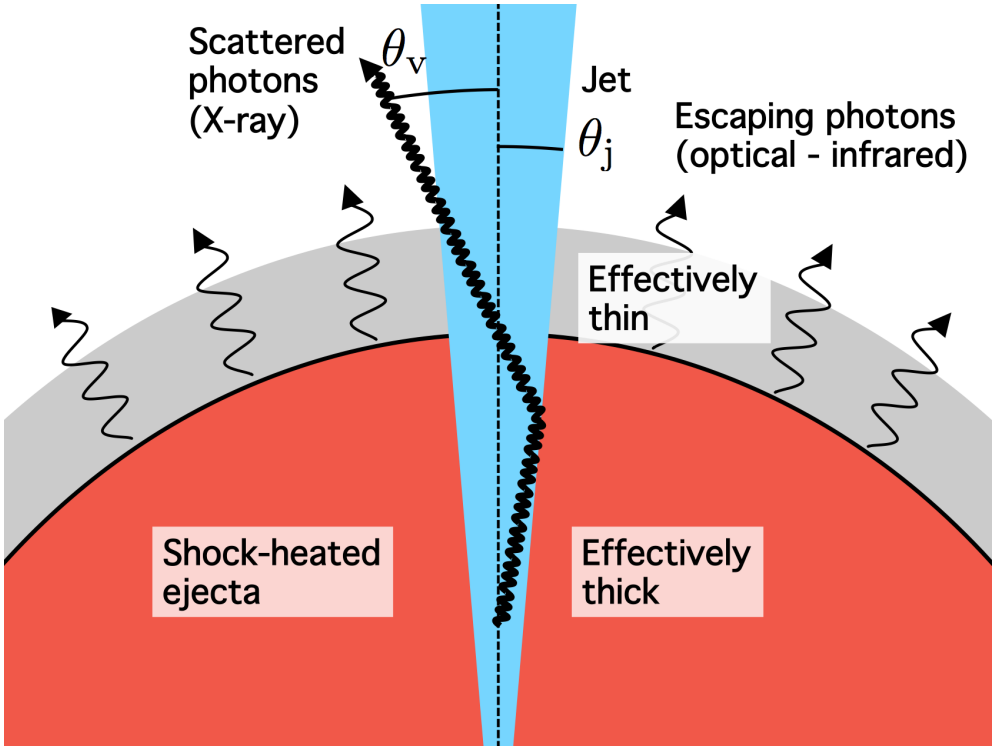

FIG. 1.— Schematic picture for the scattering of plateau emission and the engine-powered macronova. X-ray photons emitted from the inside of the jet (light blue region) are scattered by the optically thick ejecta (thick arrow). The grey region is effectively thin and the red region is effectively thick.

Big question about SGRB=NS-NS

1) All observed NS−NS binary except for one in globular cluster are within 1kpc above the disk of our Galaxy. However the observed offset of SGRB from the host galaxy is 10-100kpc, that is in the halo but not near the disk.

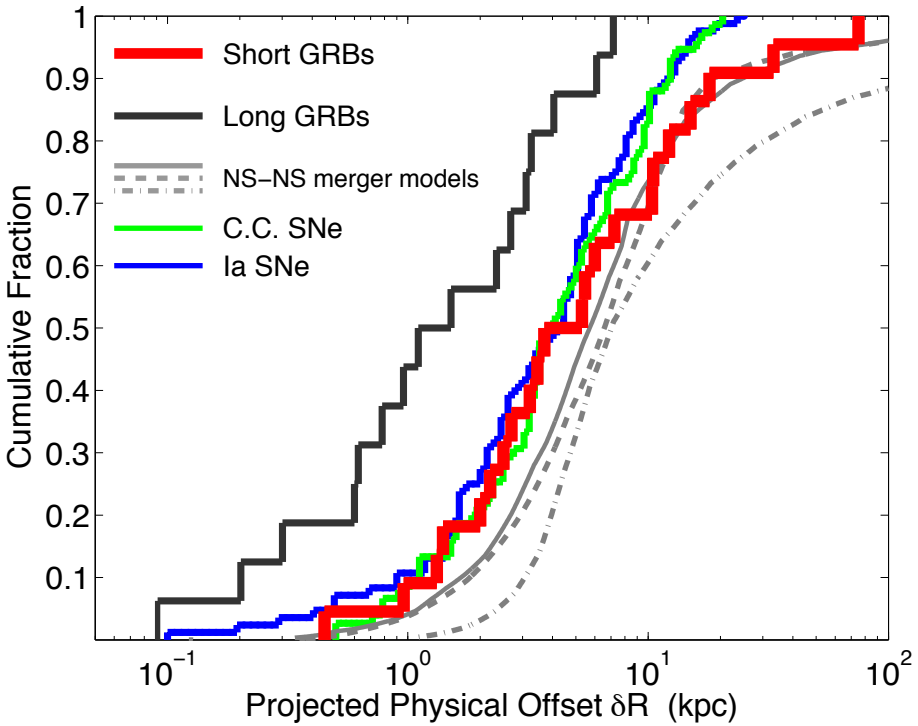

Fong & Berger 2013

2) The event rate of NS-NS merger is estimated from the observed NS-NS binary and its rate is decreasing from $83^{+209}_{-66.1}$ events/y (Kalogera et al. 2004) to 8^{+10}_{-5} events/y (Kim et al. 2015). They are using 27 different model and there is a factor 38 difference among the models. For example Kim et al. use model 6 but if they use model 1 the result is a factor 3 decreases to be ～3 events/y.

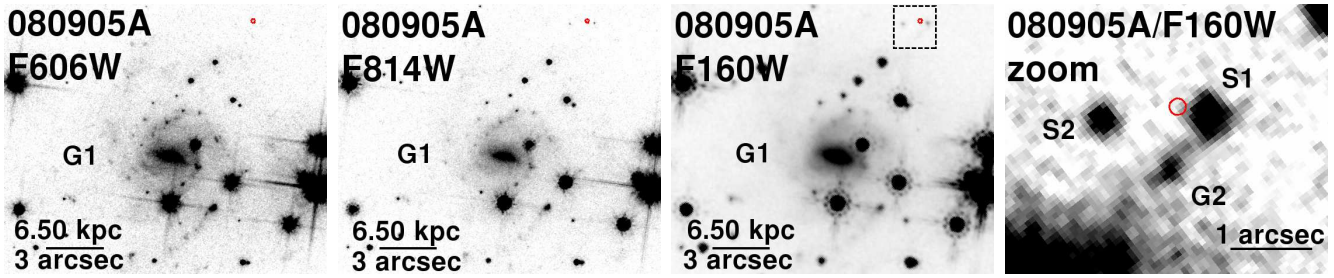

Figure 2. *HST* observations of GRB 080905A with the optical afterglow position (3σ; red circle) indicated. The face-on spiral galaxy at $z = 0.1218$, claimed as the host by Rowlinson et al. (2010b), is labeled as "G1" ($P_{cc}(< \delta R) \approx 0.01$) in each of the 3 filters, while a zoomed version of the F160W observation shows a new extended source, "G2" ($P_{cc}(< \delta R) \approx 0.08$), as well as two sources with stellar PSFs denoted as "S1" and "S2". All images are oriented with North up and East to the left.

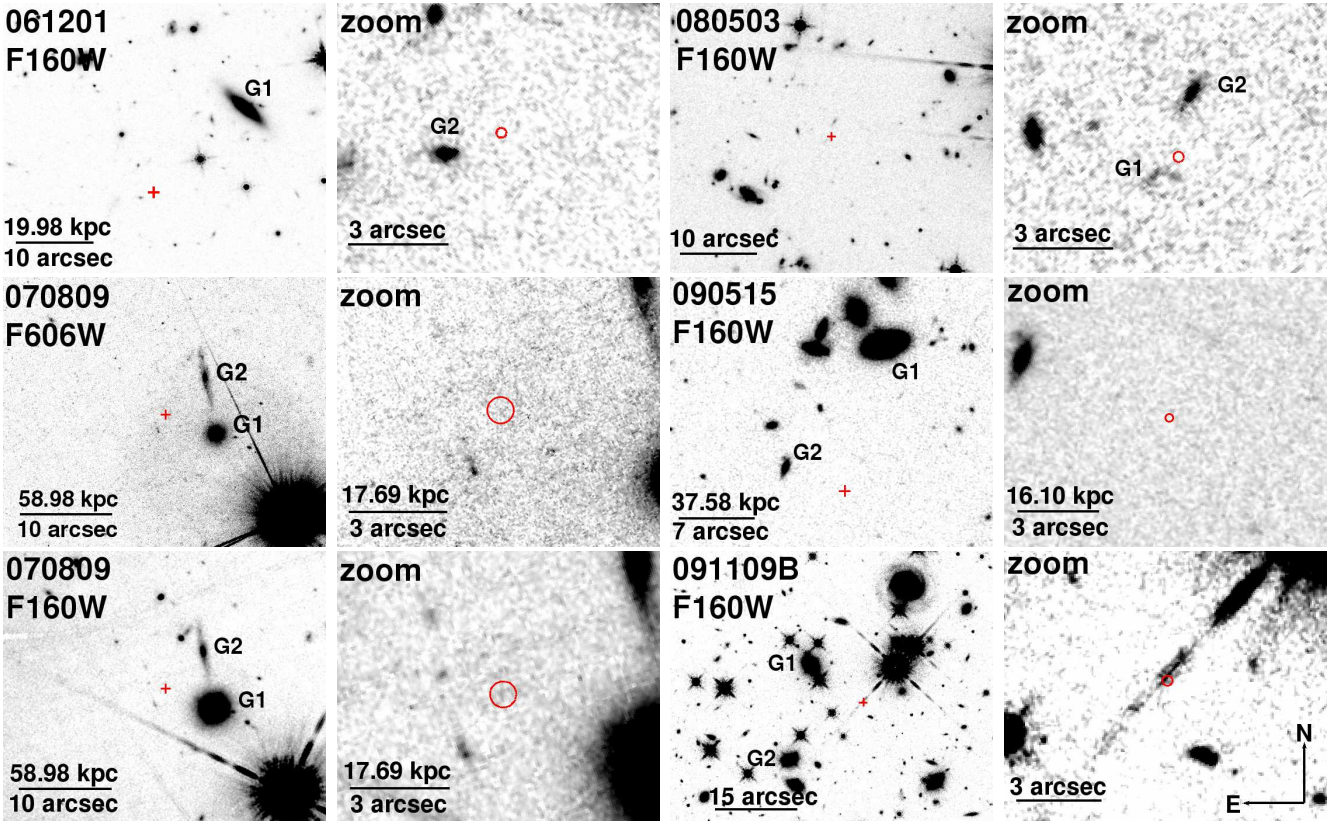

Figure 3. *HST* observations of 5 short GRBs with no coincident host galaxy to $m_{160W} \gtrsim 26.2$ mag ("host-less" bursts). We note that the afterglow position of GRB 091109B is contaminated by a diffraction spike so we place a comparatively shallow limit on a coincident host galaxy of $m_{160W} \gtrsim 25$ mag. The large-scale environments (left) and the $10''$ surrounding the afterglow position (right) are shown for each burst. The most probable and second most probable host galaxies from probability of chance coincidence analysis are labeled ("G1" and "G2", respectively). The afterglow positions are shown by the red cross or error circle in each frame. Error circles are 5σ in radius except for GRB 070809, which is 1σ because the uncertainty is based on absolute astrometry. Physical scales in kpc are based on the redshift of "G1" for each burst, if known. All images are oriented with North up and East to the left.

List of observed binary NS

Table 1
Properties of PSR–NS Binaries Considered in this Work

PSR Name	P_s (ms)	$\dot{P}_s$ 10^{-18} (ss^{-1})	M_{psr} ($M_\odot$)	M_c ($M_\odot$)	P_{orb} (hr)	e	$f_{b,obs}$	$f_{b,eff}$	τ^a_{age} (Gyr)	τ_{mgr} (Gyr)	τ_d (Gyr)	N_{psr}	C (kyr)	Ref[b]	l	b
Tight binaries																
B1913+16	59.	8.63	1.44	1.39	7.75	0.617	5.72	2.26	0.0653	0.301	4.31	576	111	1,2	49.2°	2.16°
B1534+12	37.9	2.43	1.33	1.35	10.1	0.274	6.04	1.89	0.200	2.73	9.48	429	1130	3,4	19.0°	48.0°
J0737-3039A	22.7	1.74	1.34	1.25	2.45	0.088		1.55	0.142	0.086	14.2	1403	105	5	245°	-4.2°
J0737−3039B	2770.	892.			2.45	0.088		14.	0.0493		0.039			6		
J1756−2251	28.5	1.02	1.4	1.18	7.67	0.181		1.68	0.382	1.65	16.1	664	1821	7	7.0°	-0.67°
J1906+0746	144.	20300.	1.25	1.37	3.98	0.085		3.37	0.000112	0.308	0.082	192	126	8,9	41°	-0.3°
Wide binaries															180°	54°
J1518+4904	40.94	0.028	1.56	1.05	206.4	0.249		1.94	29.2	$>\tau_H$	51.0	276	18,700	10,11	13°	0.15°
J1811−1736	104.18	0.901	1.60	1.00	451.2	0.828		2.92	1.75	$>\tau_H$	7.9	584	5860	12,13	53°	15°
J1829+2456	41.01	0.053	1.14	1.36	28.3	0.139		1.94	12.3	$>\tau_H$	43.0	271	19,000	14	6.8°	1.3°
J1753−2240[c]	95.14	0.97	*1.25*	*1.25*	327.3	0.303		2.80	1.4	$>\tau_H$	8.2	270	13,900	15		

THE ASTROPHYSICAL JOURNAL, 715:230–241, 2010 May 20 RICHARD O'SHAUGHNESSY[1] AND CHUNGLEE KIM[2]

Distance to B1534+12 is 0.7kpc so that only 778pc from galactic plane not being in the halo
Distance to J1518+14 is 0.625kpc so that only 860pc from galactic plane not being in the halo
（ArXiv.08082292）

NS-NS binaries seem to be in our galactic plane without large kick probably because of the binary(?). NS-NS might be mainly formed in globular cluster with dead pulsar
but the rate should be much larger than Kim et al.2015(～8/yr) estimate.

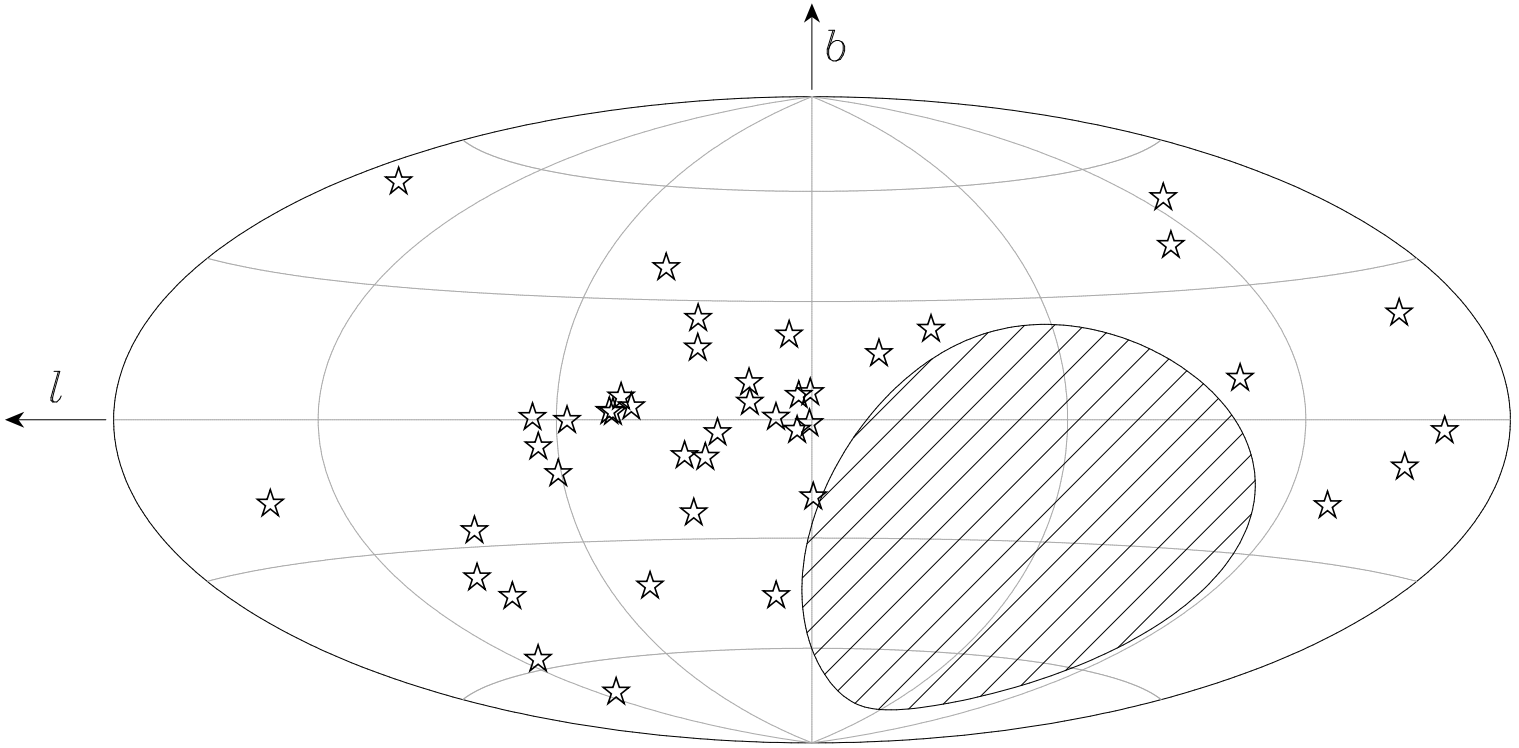

Figure 1. Distribution of the 42 MSPs, represented with a star, in Galactic coordinates (longitude l and latitude b). The center of the plot is oriented towards the Galactic Center. The hatched area is the part of the sky (declination $\delta < -39°$) that is not accessible to the EPTA.

The high galactic latitude pulsars are all near ones.

This suggests that NS-NS might have nothing to do with SGRB or, many NS-NS binary in the halo so that NS-NS rate is higher.

Conclusion

- In GWPAW2015(June) Bruce predicted GW150914 using Nakano's presentation using Kinugawa et al.2014
- Now as for chirp mass , BBH >> NS-BH >> NS-NS
- The detectable range is proportional to 5/6 power of the chirp mass and the volume is 5/2
- So that BBH is the easiest detectable source.
- Following this tendency in O2, I predict
- NS-BH will be observed !!
- I hope this slide will be shown first in GWPAW2017 like Bruce's slide in GWPAW2016.
- Within ～1year, we can know if this prediction is OK or not.